




Experimental investigation of beam-steering applied to 2×2 MIMO system with single receiving RF chain and time-modulated antenna array

Grzegorz Bogdan , Konrad Godziszewski  and Yevhen Yashchyshyn 

Warsaw University of Technology, Institute of Radioelectronics and Multimedia Technology, Nowowiejska 15/19, 00-665 Warsaw, Poland

Research Paper

Cite this article: Bogdan G, Godziszewski K, Yashchyshyn Y (2020). Experimental investigation of beam-steering applied to 2×2 MIMO system with single receiving RF chain and time-modulated antenna array. *International Journal of Microwave and Wireless Technologies* **12**, 504–512. <https://doi.org/10.1017/S1759078720000744>

Received: 31 October 2019

Revised: 8 May 2020

Accepted: 12 May 2020

First published online: 19 June 2020

Key words:

Adaptive arrays; antenna arrays; time-modulated antenna arrays; beamforming; beam-steering; multiple-input multiple-output (MIMO)

Author for correspondence:

Grzegorz Bogdan,
E-mail: g.bogdan@ire.pw.edu.pl

Abstract

Multiple antennas and multiple radio frequency (RF) chains in both the transmitter and receiver are required in conventional radio systems employing the multiple-input multiple-output (MIMO) method. This paper presents an experimental investigation of a beam-steering time-modulated MIMO receiver with a single RF chain. Implementation of the receiver is based on a time-modulated antenna array (TMAA) and a software-defined radio. The sidebands generated inherently by the TMAA are utilized as virtual spatial channels with the beam-steering functionality. Performance of the system is investigated experimentally. The bit error rate and condition number of the channel matrix are examined for different radiation patterns in order to determine favorable configurations in a given multipath environment. Obtained results show a considerable impact of the beam-steering on the performance of MIMO transmission.

Introduction

It is anticipated that future wireless systems will extensively utilize two main multi-antenna techniques, i.e. the multiple-input multiple-output (MIMO) and the beamforming [1]. MIMO is commonly used to increase the capacity of a wireless channel by exploiting the spatial properties of a multipath environment; therefore, it is dedicated for non-line-of-sight (NLOS) conditions. In contrast, the beamforming is usually used to improve the gain in the line-of-sight (LOS) propagation. The beamforming can be realized with a phased antenna array (PAA) [2], a reconfigurable aperture [3], or a digital signal processing. It can be also obtained with a time-modulated antenna array (TMAA) which is considered as an unconventional beamforming architecture [4]. The TMAA concept was first proposed in 1959 [5] as an alternative to the PAA because fast radio frequency (RF) switching allows similar weighting of RF signals and switches have several advantages over phase shifters [6]. However, in contrast to the PAA, output signal of the TMAA is spread into multiples of the modulation frequency around the center frequency. This phenomenon used to be considered as a disadvantage; therefore, many suppressing techniques have been proposed in the literature [7–9]. Nowadays, the peculiar properties of the sidebands are considered as useful in many applications, e.g. beam-steering [10], spatial multiplexing [11], direction finding [12], MIMO radar [13], or MIMO communication [14]. In addition, the sidebands inherently generated by the TMAA can be utilized as virtual transmission channels in multipath scenarios [15]. This approach was employed to devise a maximum ratio combiner [16], a compact single-RF MIMO receiver [17], and the beam-steering time-modulated MIMO (BS-TM-MIMO) receiver [18]. Implementation of a wideband BS-TM-MIMO receiver, which supports processing of wideband signals up to 50 MHz, was presented in [19]. In this paper, which is a follow-up of [18] and [19], we present an extended experimental investigation of the BS-TM-MIMO receiver operating indoor in a multipath propagation environment.

Time-modulated antenna array

Theoretical fundamentals

TMAAs are commonly referred to as 4D arrays, because time is utilized as an additional degree of freedom for beamforming. The time modulation is typically based on fast and periodic ON/OFF keying. In result, the beamforming and beam-steering, which have been traditionally related to PAAs, can be realized without phase-shifters. Various types of TMAAs were extensively elaborated in many scientific publications [4–28]; therefore, only a brief introduction to this topic will be provided in this paper. Properties of the TMAA will be described in the receiving mode without losing the generality. [Figure 1](#) shows a typical configuration of a

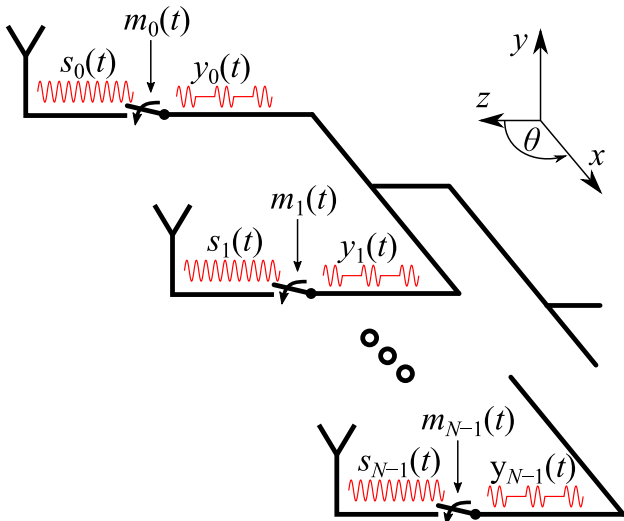


Fig. 1. Diagram of a linear TMAA with SPST switches.

linear TMAA with a uniform spacing between elements distributed along the x -axis and SPST (single-pole single-throw) RF switches incorporated into a feed network. Figure 2 illustrates corresponding modulating functions, which are also referred to as switching sequences.

RF switches modulate (by means of a periodic ON/OFF keying) signals $s_n(t)$ delivered from each antenna, where $n = 0 \dots N-1$ is the index of the antenna and N is the total number of antennas in the array. Operation of each switch can be expressed as a modulation of $s_n(t)$ by function $m_n(t)$, which is periodic and associate value of “0” for OFF and “1” for ON. All modulating functions share the same modulation frequency $f_0 = 1/T_0$, where T_0 is the period of modulation. Two constrains must be satisfied [20]:

- (1) the modulation frequency must be much smaller than the carrier frequency of an RF signal ($f_0 \ll f_c$),
- (2) the modulation frequency must be greater than the bandwidth of an RF signal ($f_0 > B$).

The TMAA array factor can be formulated as [4]:

$$AF(\theta, t) = \sum_{n=0}^{N-1} m_n(t) S_n e^{jkn d \sin \theta}, \tag{1}$$

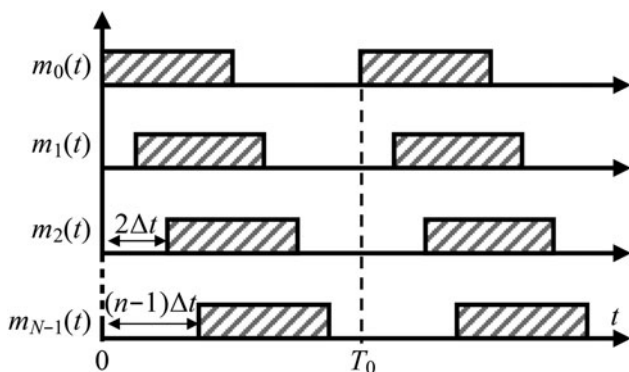


Fig. 2. Unipolar switching sequences.

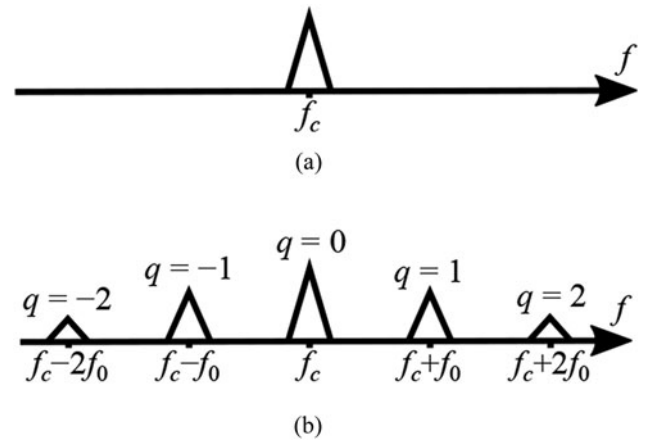


Fig. 3. Spectrum of the signal (a) impinging upon TMAA; (b) at the output of TMAA.

where S_n represents the complex excitation, d is the distance between antenna elements in the array, θ is the angle, and $k = 2\pi/\lambda$ is the wave number. Due to its periodicity, $m_n(t)$ can be expressed in terms of a sum of complex Fourier series coefficient $M_n^{(q)}$:

$$m_n(t) = \sum_{q=-\infty}^{\infty} M_n^{(q)} e^{jq\omega_0 t} \tag{2}$$

$$M_n^{(q)} = \frac{1}{T_0} \int_{-T_0/2}^{T_0/2} m_n(t) e^{-jq\omega_0 t} dt, \tag{3}$$

where $\omega_0 = 2\pi/T_0$ and $q \in (-\infty, \infty)$. After substituting (2) into (1), the time-dependency is converted to the frequency-dependency and the array factor can be formulated as follows:

$$AF(\theta) = \sum_{n=0}^{N-1} S_n M_n^{(0)} e^{jkn d \sin \theta} + \sum_{\substack{q=-\infty \\ q \neq 0}}^{\infty} \sum_{n=0}^{N-1} S_n M_n^{(q)} e^{jkn d \sin \theta} e^{jq\omega_0 t}. \tag{4}$$

According to (4), the time-modulated signal is composed of a central component ($q = 0$) and sideband components ($q \in \mathbb{Z}, q \neq 0$). The latter are placed on multiples of modulation frequency around the center frequency. Figure 3 presents an example of a bandpass signal’s spectrum before (Fig. 3(a)) and after (Fig. 3(b)) time modulation. It shows that the sidebands are in fact spectral replicas of the original signal; however, they demonstrate different spatial properties because each sideband carries information received at frequency f_c from a different angle [11]. Therefore, sidebands can be utilized as diverse transmission channels [14–19].

Values of complex Fourier coefficients $M_n^{(q)}$ in (4) can be modified by adjusting the ON and OFF times of modulating functions. The beam-steering is obtained when switches are turned ON and OFF sequentially with some fixed delay with respect to the preceding one [21]. Hence, operation of the n -th switch is

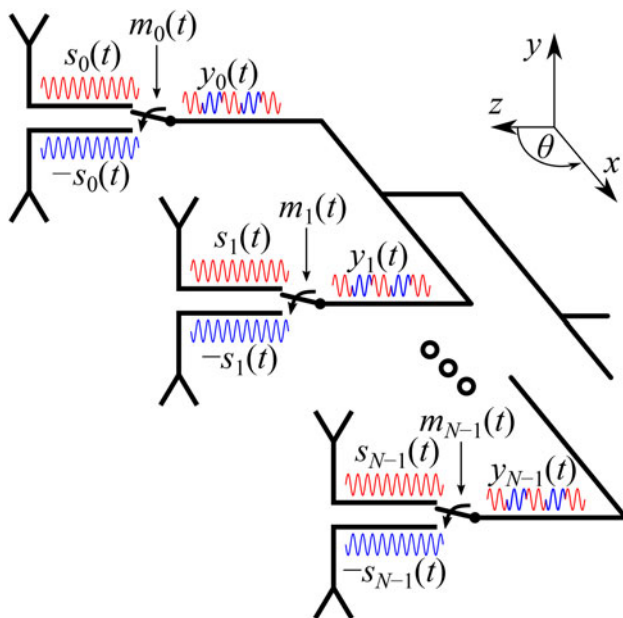


Fig. 4. Diagram of TMAA with SPDT switches connected to oppositely oriented antennas.

related to the operation of the first switch in the following way:

$$m_n(t) = m_0(t - n\Delta t), \tag{5}$$

where Δt is the delay progression. According to the time-shift property of the Fourier transform, the delay progression alters the phase of the Fourier coefficients as follows:

$$m_n(t - n\Delta t) \overset{\mathfrak{F}}{\Leftrightarrow} M_0^{(q)} e^{-\frac{j2\pi q n \Delta t}{T_0}}, \tag{6}$$

hence enables beamforming similarly to PAAs.

Design

The very first prototype of the TMAA was presented in 1963 [22]. It was based on p-i-n diodes used as switches and demonstrated 10 kHz of the maximum signal bandwidth. Since then, over the last 50 years of progress in electronics and semiconductor technology, advanced switching devices with cutting edge performance have become available off-the-shelf. Moreover, more functional TMAA architectures with improved efficiency were proposed. For instance, the TMAA in [9] uses the I/Q channel modulator which is composed of two Wilkinson power dividers, two RF switches, two $0/\pi$ phase shifters in RF channels, and one $\pi/2$ fixed-phase shifter in the control circuit to realize a single-sideband time-modulated phase-only weighting. In [23], a less complex TMAA was presented because the $0/\pi$ phase shifters were avoided. Instead, a linear antenna array was complemented by identical, however, oppositely oriented antenna array and single-pole double-throw (SPDT) switches were used to alternate signals between elements of these two arrays as illustrated in Fig. 4. Such a design can be considered as a special case of the TMAA with bipolar squared periodic sequences [24].

Each n -th pair of the oppositely oriented antennas can be treated as a single element of the linear array. Therefore, its radiation

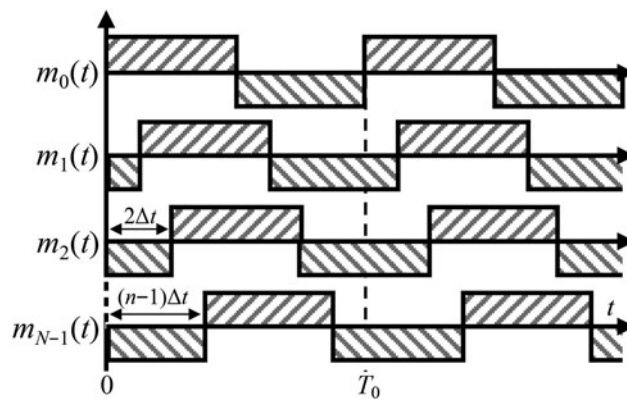


Fig. 5. Bipolar switching sequences.

pattern in xz -plane can be calculated with equation (4). However, the Fourier coefficients $M_n^{(q)}$ have to be computed for the bipolar switching sequences presented in Fig. 5.

The design of the TMAA used in the experiments is presented in Fig. 6. Details on the design and specification can be found in [25]. The TMAA is composed of two layers: a superstrate with the permittivity of 2.2 (RT/duroid588) and a substrate with the permittivity of 3.66 (RO4003C). A single element of the array is composed of two oppositely oriented series-fed double-patch antennas. The elements are electromagnetically coupled with microstrip lines, which are connected to the throws of SPDT switches. The elements are designed for the center frequency of 5.6 GHz. Four elements are arranged in the form of a linear array.

The RF switches ADRF5020 [26] are incorporated into the feed network. This particular model was selected because of its ultrashort switching time of 2 ns and a very good microwave performance at 5.6 GHz. The switching is periodic with repetition frequency $f_0 = 50$ MHz, or equivalently the repetition period of 20 ns. It is also uniform, i.e. each antenna in pair is active for $0.5T_0$. The digital delay lines 3D3438 [27] are used to introduce delays between switching sequences. A step of the delay applied to switching sequences equals 60 ps which corresponds to $0.003T_0$.

The total efficiency of the TMAA (η_T) can be estimated by taking into account the radiation efficiency (η_R), the switching

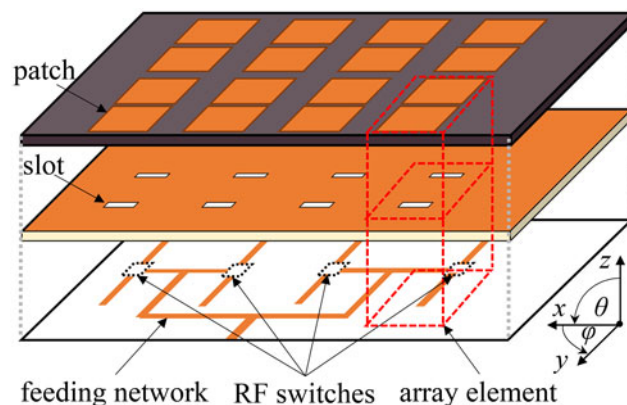


Fig. 6. Design of the TMAA.

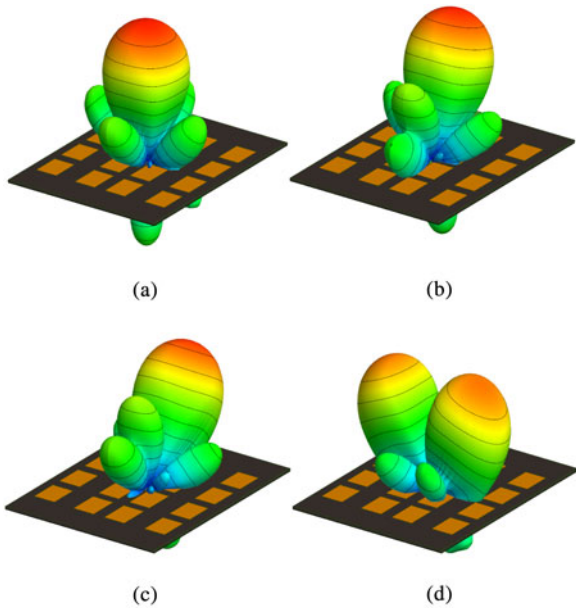


Fig. 7. Antenna patterns of TMAA simulated for (a) $q = -1$ and $\Delta t = 0$, (b) $q = -1$ and $\Delta t = 0.15T_0$, (c) $q = -1$ and $\Delta t = 0.28T_0$, (d) $q = 0$.

efficiency (η_s), and the harmonic efficiency (η_H) [28]. The radiation efficiency was estimated at 0.6 by considering the radiation efficiency of the antenna structure computed with an electromagnetic simulator and the insertion loss of the switch. The switching efficiency can be estimated at 1, because the SPDT switches always connect an element of the array to the feed network. Hence, the power of an RF signal is not dissipated in the matched load during the OFF state. The harmonic efficiency depends on the switching sequence and corresponding magnitudes of harmonics, according to:

$$\eta_H^{(q)} = |M_n^{(q)}|^2 / \sum_{k=-\infty}^{\infty} |M_n^{(k)}|^2. \tag{7}$$

Magnitudes of the harmonics are obtained after expressing the switching sequence in terms of the Fourier series. For example, magnitudes of the central component and the first negative harmonic for unipolar switching sequences presented in Fig. 2 equal $|M_n^{(0)}| = 0.5$ and $|M_n^{(-1)}| = 0.3183$, respectively. In our case, the TMAA is controlled by bipolar switching sequences presented in Fig. 5; hence the opposite antennas are excited with symmetrical unipolar RF pulses. Therefore, the harmonic efficiency obtained from (7) should be multiplied by two. This yields the harmonic efficiency of $\eta_H^{(0)} = 0.5$ and $\eta_H^{(-1)} = 0.2$ for the central component and the first negative harmonic, respectively. If the RF system is capable of processing multiple spectral components, then the harmonic efficiency is a sum of efficiencies calculated for each. For example, if both the central component and the first negative sideband component are processed, then the harmonic efficiency $\eta_H = \eta_H^{(-1)} + \eta_H^{(0)} = 0.7$. Therefore, the total efficiency of the TMAA for MIMO can be estimated at $\eta_T = \eta_R \eta_s \eta_H = 0.42$.

Figures 7(a)–7(c) show partial antenna patterns simulated for the first negative sideband ($q = -1$) and different values of the delay progression Δt . The beam-steering is performed in xz -plane. Figure 7(d) shows the antenna pattern at the central component

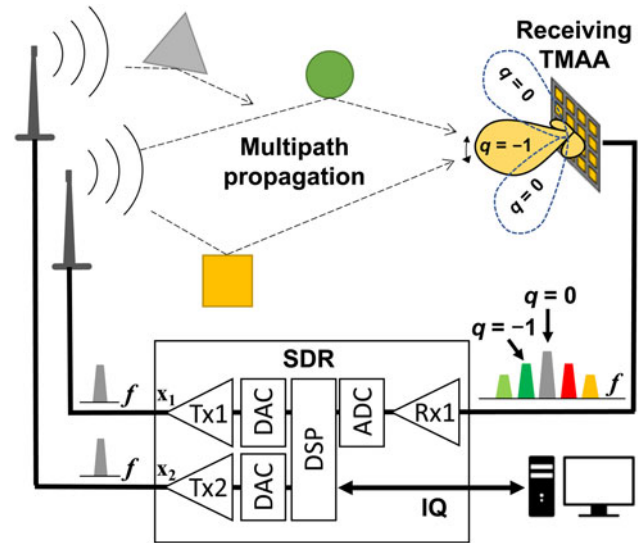


Fig. 8. Diagram of the BS-TM-MIMO.

($q = 0$). It is divided by a deep broadside null into two beams, which are directed toward -24° and $+24^\circ$ in yz -plane. Comparing Figs 7(a)–7(d) one can observe that the antenna patterns simulated over the first negative sideband and the central component are complementary.

Concept and properties of BS-TM-MIMO

System design

Diagram of the 2×2 BS-TM-MIMO concept is presented in Fig. 8. The transmitting part resembles a regular 2×2 MIMO transmitter, i.e. two streams of symbols x_1 and x_2 are up-converted and sent from transmitting RF chains (Tx1 and Tx2) via omnidirectional dipole antennas. Waves transmitted from omnidirectional antennas propagate inside a multipath environment. The receiving part is modified with respect to a conventional 2×2 MIMO receiver in two ways. Firstly, only one receiving RF chain is used instead of two. Secondly, a single TMAA with the beam-steering is used instead of two separate antennas. This modification leads to a more compact and less power consuming design; however, a wider frequency band must be processed in the receiving RF chain. These modifications are possible, because TMAA converts spatial diversity into frequency diversity, i.e. combinations of waves approaching from different directions are available on different frequencies. For instance, waves approaching from xz -plane are available on odd sidebands ($q = \pm 1, \pm 3, \pm 5, \dots$) and waves approaching from yz -plane (excluding the broadside direction) are available at the center frequency ($q = 0$). Sidebands are demultiplexed in the baseband for further processing as diverse transmission channels.

Antenna pattern impact on MIMO performance

Two main requirements should be satisfied for an effective MIMO transmission. Firstly, a level of the signal to noise ratio (SNR) must be sufficiently high to correctly demodulate received symbols. Secondly, received signals should not be correlated. A level of the SNR can be increased by using directional antennas

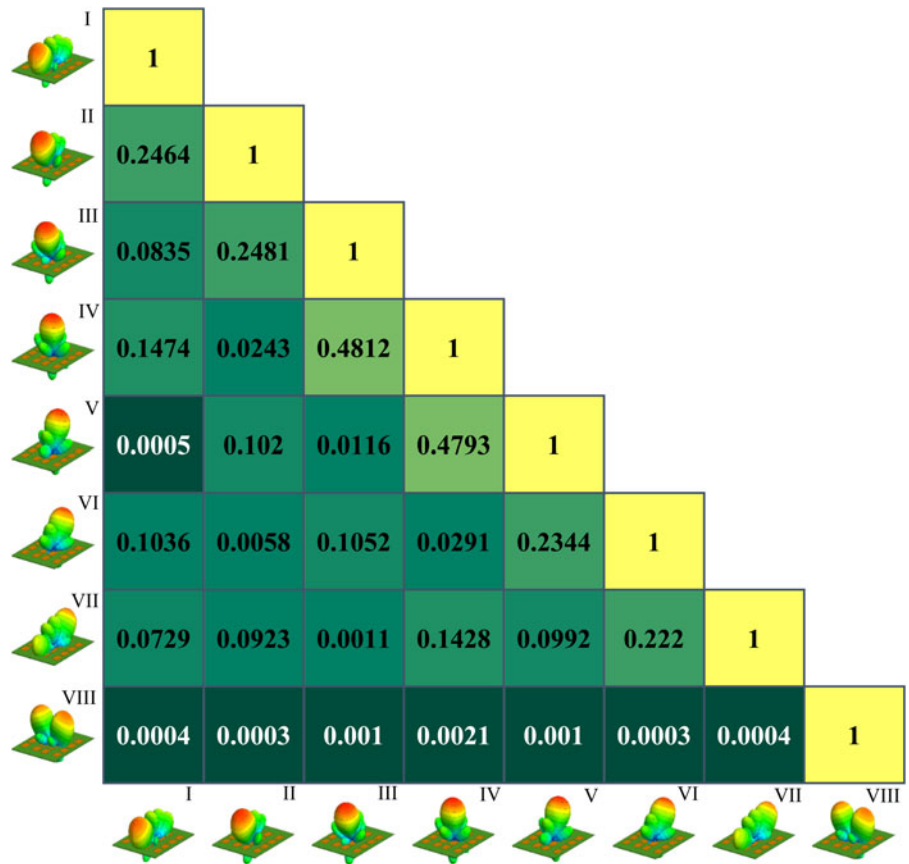


Fig. 9. ECC calculated for different pairs of TMAA antenna patterns.

which provide higher gain than omnidirectional antennas, therefore can compensate for the path loss of a radio channel. Nevertheless, directional antennas reduce the angular spread of the channel, thus decrease the MIMO performance. Another solution is an adaptive antenna with a controllable pattern. Its beam can be focused toward a direction which provides a signal with high SNR and satisfactory multipath richness.

The requirement of a low correlation between spatial streams can be satisfied to some degree when antennas are dislocated on more than a quarter of the wavelength [29]. Otherwise, the performance of MIMO may be significantly limited. The necessary diversity can be produced with distinct antenna patterns, i.e. highly orthogonal patterns create a low correlation, hence capacity gains are possible [30, 31]. Correlation between two

antenna patterns can be expressed with an envelope correlation coefficient (ECC) [32]

$$ECC = \frac{\left| \iint \vec{F}_1(\theta, \varphi) \cdot \vec{F}_2^*(\theta, \varphi) d\Omega \right|^2}{\iint |\vec{F}_1(\theta, \varphi)|^2 d\Omega \iint |\vec{F}_2(\theta, \varphi)|^2 d\Omega}, \quad (8)$$

where $\vec{F}_i(\theta, \varphi)$ is the pattern of the i -th antenna. Value of the ECC ranges from <0.1 for low correlation to ~ 0.5 for the nominal, and >0.9 for the high correlation [33]. Figure 9 shows the ECC calculated for different pairs of TMAA antenna patterns. As given in Table 1, the patterns indicated with roman numbers from I to VII were simulated for the first negative sideband

Table 1. Direction of the main beam in terms of the elevation (θ) and azimuthal angles (φ) obtained for different TMAA configurations.

Pattern no.	q	Δt	θ	φ
I	-1	0.441	45°	0°
II	-1	0.288	30°	0°
III	-1	0.144	15°	0°
IV	-1	0	0°	0°
V	-1	-0.144	-15°	0°
VI	-1	-0.288	-30°	0°
VII	-1	-0.441	-45°	0°
VIII	0	Any	24°	$\pm 90^\circ$

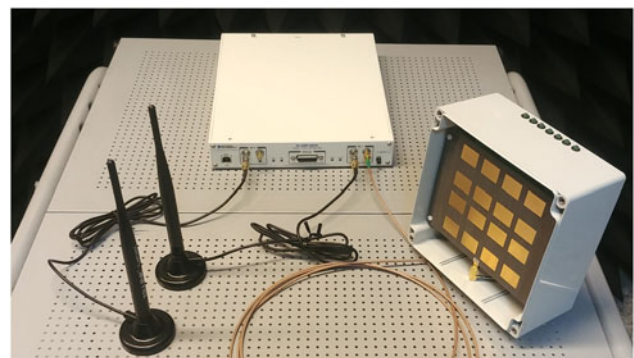


Fig. 10. Experimental setup composed of two dipole antennas, SDR, and the TMAA.

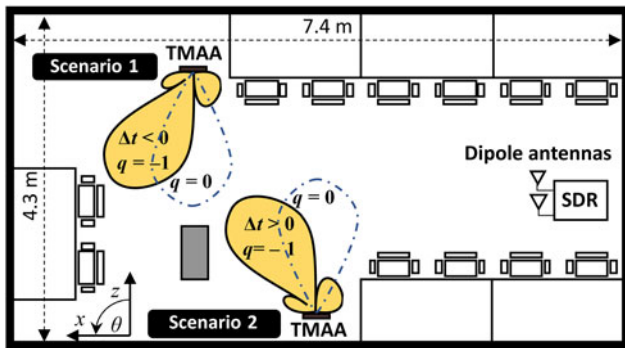


Fig. 11. Experimental scenarios.

component ($q = -1$) and different Δt . Pattern VIII was simulated for the central component ($q = 0$). The lowest values of the ECC are obtained when pattern VIII is combined with any other, because of its divergent shape. In many applications, pattern VIII could be recognized as disadvantageous; however, in MIMO system, it can provide better diversity.

The ECC is a popular metric indicating the effectiveness of MIMO antennas; however, it does not consider the characteristic of a multipath environment. In practical cases, a condition number (κ) of the channel matrix is a more reliable indicator of the correlation between spatial streams. The condition number is calculated from the instantaneous channel matrix \mathbf{H} without the need for stochastic averaging [34] according to:

$$\kappa = 20 \log_{10}(\hat{\mathbf{H}}\hat{\mathbf{H}}^{-1}) \quad (\text{dB}) \quad (9)$$

where $\hat{\mathbf{H}}$ is an estimate of the channel matrix. A well-conditioned channel matrix indicates a low correlation between received signals and yields a low value of the condition number, which facilitates MIMO communication in the high SNR regime [35]. Such a condition is usually obtained in NLOS propagation when the LOS wave is significantly attenuated.

Experimental investigation

The experimental 2×2 spatial multiplexing MIMO setup is presented in Fig. 10. A software-defined radio (SDR) with two full-duplex wideband transceivers was used as the RF front-end. Both transceivers cover frequencies from 10 MHz to 6 GHz with 160 MHz of analogue bandwidth. In addition, they are coherent and phase-aligned which facilitate the development of MIMO applications [36]. Two transmitting RF chains of the SDR were configured to upconvert and transmit the quadrature phase shift keying symbols at 5.6 GHz via two dipole antennas. A single receiving RF chain of the SDR was configured to downconvert and sample a wideband signal from the TMAA in a frequency range 5.5–5.7 GHz. This band included the first negative sideband component at 5.55 GHz, the central component 5.6 GHz, and the first positive sideband component at 5.65 GHz. The central component ($q = 0$) and the first negative sideband component ($q = -1$) were selected for further processing because, according to Fig. 9, antenna patterns related to these components give the lowest ECC. More details about the setup can be found in [19].

The primary purpose of the experimental investigation was to make a qualitative evaluation of the BS-TM-MIMO receiver operating in a typical indoor environment. Performance of the

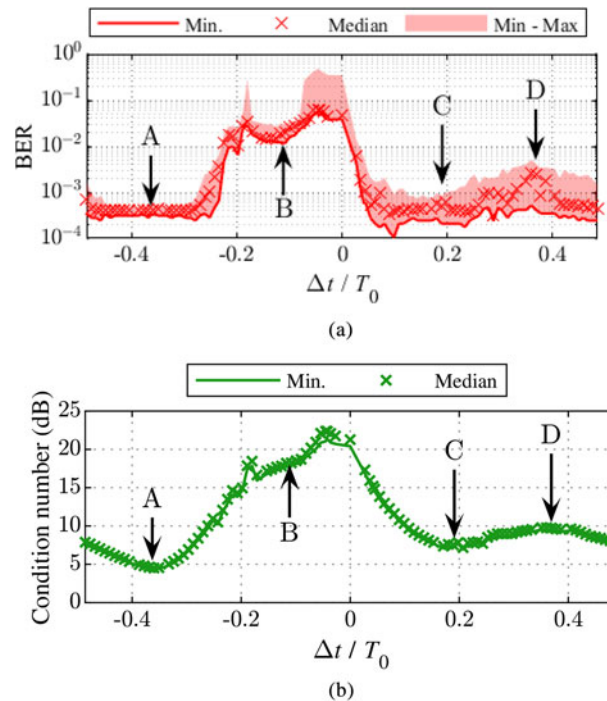


Fig. 12. Scenario 1 (a) BER; (b) condition number.

receiving system was assessed by calculating two fundamental metrics: the bit error rate (BER) and the condition number of the channel matrix. The experiments were conducted inside a room with tables, chairs, and desktop computers located next to the walls. The plan of the room is presented in Fig. 11. Two transmitting dipole antennas were located 0.6 m above the floor and 1.2 m beside the wall. The distance between dipole antennas was $22 \text{ cm} \approx 4\lambda$. The experiments were conducted in various locations, although in this paper, we only discuss the results of the two most representative cases which are designated in Fig. 11 as Scenario 1 and Scenario 2. In both scenarios, the MIMO transmission was assessed in 101 different configurations. In all of the configurations, the central component pattern was fixed; although different antenna patterns were configured over the first negative sideband ($q = -1$), i.e. the main beam was steered from -50° to $+50^\circ$. In addition, each configuration was tested 100 times in order to obtain statistically reliable data. Experiments were conducted in a non-isolated environment, hence the transmission was subject to spontaneous interferences from wireless local area networks (e.g. IEEE 802.11n/ac) operating in 5 GHz band. Therefore, in order to remove corrupted data, the frames of which the BER was 10 times higher than the minimum value obtained in a given configuration were removed.

Figure 12(a) shows the minimum, the median, and the minimum to maximum range of the BER measured in Scenario 1 for different configurations of the TMAA ($-0.468T_0 < \Delta t < 0.468T_0$). Figure 12(b) presents the condition number calculated in each configuration. Annotations of Figs 12(a)–12(d) designate four representative cases. The antenna patterns and the in-phase and quadrature (IQ) samples for these cases are presented in Figs 13 and 14, respectively. If Δt is negative, then the main beam is directed away from the transmitting dipoles as presented in Fig. 11.

Hence, the LOS component is significantly attenuated, and the received signal is mainly a combination of waves reflected from

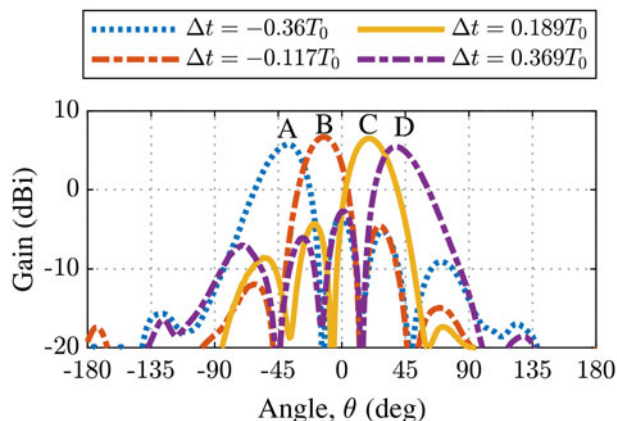


Fig. 13. Antenna patterns at the first negative sideband ($q = -1$) for selected TMAA configurations.

objects and walls of the room. Despite the fact that the signal power level is relatively low, the BER remains stable on a low level around 3×10^{-4} for $\Delta t < -0.261T_0$. This indicates good performance of MIMO and low correlation of streams, which is also confirmed by a low value of the condition number $\kappa = 4.5$ dB in configuration A. In case B ($\Delta t = -0.117T_0$), the main beam is directed toward a corner of the room behind a pillar which is hardly reachable by reflections. According to Fig. 14(b), the amplitude of symbols is smaller compared to Fig. 14(a) which indicates lower power of the received signal and leads to degradation of the BER. High value of the condition number ($\kappa > 15$ dB) indicates that the channel matrix is ill-conditioned, i.e. LOS component is dominating, although weak because it is received by a sidelobe. The median of the BER recovers for $\Delta t = 0.036T_0$. It remains stable around 5×10^{-4} , however the

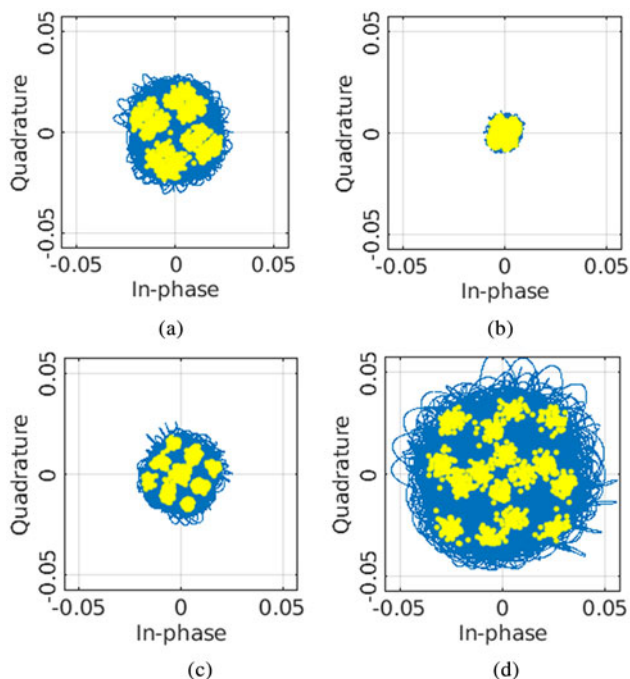


Fig. 14. IQ samples obtained from the first negative sideband ($q = -1$) for (a) $\Delta t = -0.36T_0$; (b) $\Delta t = -0.117T_0$; (c) $\Delta t = 0.189T_0$; (d) $\Delta t = 0.369T_0$.

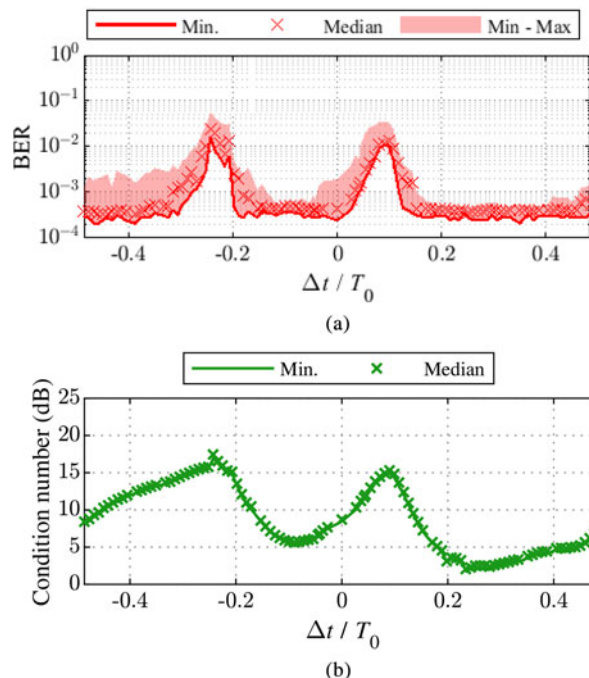


Fig. 15. Scenario 2 (a) BER; (b) condition number.

minimum to maximum range is extended. In case C ($\Delta t = 0.189T_0$), the main beam is directed toward 20° . Hence, the received signal is mainly composed of strong reflections from oppositely located objects and the wall. The power of received signal increases for $\Delta t > 0.189T_0$ because the main beam is moving toward the direction of transmitting dipoles. Nevertheless, in case D ($\Delta t = 0.369T_0$), when the main beam is directed toward 40° , despite the high signal level (Fig. 14(d)), both the BER and the condition number increase noticeably. This effect is most probably a consequence of a more significant role of the LOS component against NLOS multipaths.

In Scenario 2, the TMAA was placed on the opposite side of the room as shown in Fig. 11. Obtained values of the BER and condition number are presented in Fig. 15. The results correspond to observations and conclusion drawn for Scenario 1.

Conclusion

Experimental results presented in this paper show the performance of the 2×2 MIMO receiver based on the TMAA and a single RF chain. Two spectral replicas generated inherently by the TMAA were effectively used instead of two conventional antennas with separate RF chains. Diversity of the spectral replicas was obtained by the spatial orthogonality of the antenna patterns. The beam-steering functionality of the TMAA was used to adapt to a multipath environment. Results of the conducted experiments show that the TMAA can be used to decrease the condition number of a channel matrix, hence, to reduce the number of transmission errors which leads to an improved performance of a 2×2 MIMO system.

Acknowledgement. This work was supported by the Faculty of Electronics and Information Technology, Warsaw University of Technology under grant number IRiTM/2018/9.

References

1. Alexiou A and Haardt M (2004) Smart antenna technologies for future wireless systems: trends and challenges. *IEEE Communications Magazine* **42**, 90–97.
2. Mailloux RJ (2005) *Phased Array Antenna Handbook*. Boston: Artech House.
3. Yashchyshyn Y, Derzakowski K, Bogdan G, Godziszewski K, Nyzovets D, Kim CH and Park B (2018) 28 GHz switched-beam antenna based on s-pin diodes for 5 G mobile communications. *IEEE Antennas and Wireless Propagation Letters* **17**, 225–228.
4. Rocca P, Oliveri G, Mailloux RJ and Massa A (2016) Unconventional phased array architectures and design methodologies – a review. *Proceedings of the IEEE* **104**, 544–560.
5. Shanks HE and Bickmore RW (1959) Four-dimensional electromagnetic radiators. *Canadian Journal of Physics* **37**, 263–275.
6. Yashchyshyn Y, Godziszewski K, Bogdan G and Piasecki P (2017) X-band antenna array for low-cost beam scanning. *IET Microwaves, Antennas & Propagation* **11**, 2174–2178.
7. Drysdale TD, Allen B and Okon E (2017) Sinusoidal time-modulated uniform circular array for generating orbital angular momentum modes. *11th European Conference on Antennas and Propagation (EUCAP)*, Paris, pp. 973–977.
8. Poli L, Rocca P and Massa A (2012) Sideband radiation reduction exploiting pattern multiplication in directive time-modulated linear arrays. *IET Microwaves, Antennas & Propagation* **6**, 214–222.
9. Yao AM, Wu W and Fang DG (2015) Single-sideband time-modulated phased array. *IEEE Transactions on Antennas and Propagation* **63**, 1957–1968.
10. Poli L, Rocca P, Oliveri G and Massa A (2011) Harmonic beamforming in time-modulated linear arrays. *IEEE Transactions on Antennas and Propagation* **59**, 2538–2545.
11. Rocca P, Zhu Q, Bekele E, Yang S and Massa A (2014) 4-D Arrays as enabling technology for cognitive radio systems. *IEEE Transactions on Antennas and Propagation* **62**, 1102–1116.
12. He C, Cao A, Chen J, Liang X, Zhu W, Geng J and Jin R (2018) Direction finding by time-modulated linear array. *IEEE Transactions on Antennas and Propagation* **66**, 3642–3652.
13. Ni D, Yang S, Chen Y and Guo J (2017) A study on the application of subarrayed time-modulated arrays to MIMO radar. *IEEE Antennas and Wireless Propagation Letters* **16**, 1171–1174.
14. Rocca P, Poli L, Bekele ET and Massa A (2012) Time-modulation for MIMO systems – potentials and trends. *6th European Conference on Antennas Propagation (EuCAP)*, Prague, pp. 3285–3286.
15. Maneiro-Catoira R, Brégains J, García-Naya JA and Castedo L (2015) Time-modulated arrays for digital communications in multipath scenarios. *IEEE International Symposium On Antennas Propagation USNC/URSI National Radio Science Meeting*, Vancouver, pp. 816–817.
16. Maneiro-Catoira R, Brégains JC, García-Naya JA, Castedo L, Rocca P and Poli L (2017) Performance analysis of time-modulated arrays for the angle diversity reception of digital linear modulated signals. *IEEE Journal of Selected Topics in Signal Processing* **11**, 247–258.
17. Gwak D, Sohn I and Lee SH (2015) Analysis of single-RF MIMO receiver with beam-switching antenna. *ETRI Journal* **37**, 647–656.
18. Bogdan G, Godziszewski K, Yashchyshyn Y and Kozłowski S (2019) Single RF chain MIMO receiver using beam-steering time modulated antenna array. *13th European Conference on Antennas Propagation (EuCAP)*, Kraków, pp. 1–4.
19. Bogdan G, Godziszewski K and Yashchyshyn Y (2019) MIMO receiver with reduced number of RF chains based on 4D array and software defined radio. *27th European Signal Processing Conference (EUSIPCO)*, A Coruna, pp. 1–4.
20. Maneiro-Catoira R, Brégains JC, García-Naya JA and Castedo L (2014) On the feasibility of time-modulated arrays for digital linear modulations: a theoretical analysis. *IEEE Transactions on Antennas and Propagation* **62**, 6114–6122.
21. Bogdan G, Bajurko PR and Yashchyshyn Y (2014) Null-steering in two-element time modulated linear antenna array through pulse-delay approach. *20th International Conference on Microwaves, Radar and Wireless Communication (MIKON)*, Gdańsk, pp. 1–4.
22. Kummer W, Villeneuve A, Fong T and Terrio F (1963) Ultra-low side-lobes from time-modulated arrays. *IEEE Transactions on Antennas and Propagation* **11**, 633–639.
23. Bogdan G, Yashchyshyn Y and Jarzynka M (2016) Time-modulated antenna array with lossless switching network. *IEEE Antennas and Wireless Propagation Letters* **15**, 1827–1830.
24. Maneiro-Catoira R, Brégains JC, García-Naya JA and Castedo L (2019) Time-modulated phased array controlled with nonideal bipolar squared periodic sequences. *IEEE Antennas and Wireless Propagation Letters* **18**, 407–411.
25. Bogdan G, Godziszewski K, Yashchyshyn Y, Kim CH and Hyun S (2019) Time modulated antenna array for real-time adaptation in wide-band wireless systems – part 1: design and characterization. *IEEE Transactions on Antennas and Propagation*. Available at <https://ieeexplore.ieee.org/document/8657780> (Accessed 29 May 2020).
26. Analog Devices: ADRF5020 – 100 MHz to 30 GHz, silicon SPDT switch, Rev. A. Available at <http://www.analog.com/media/en/technical-documentation/data-sheets/ADRF5020.pdf> (Accessed 1 April 2020).
27. Data Delay Devices (2010) Monolithic 8-bit programmable delay line (series 3d3438). Available at <http://www.datadelay.com/datasheets/3d3438.pdf> (Accessed 29 May 2020).
28. Chen Q, Zhang J, Wu W and Fang D (2020) Enhanced single-sideband time-modulated phased array with lower sideband level and loss. *IEEE Transactions on Antennas and Propagation* **68**, 275–286.
29. Foschini GJ and Gans MJ (1998) On limits of wireless communications in a fading environment when using multiple antennas. *Wireless Personal Communications* **6**, 311–335.
30. Jensen MA and Wallace JW (2004) A review of antennas and propagation for MIMO wireless communications. *IEEE Transactions on Antennas and Propagation* **52**, 2810–2824.
31. Saunders S and Aragón-Zavala A (2007) *Antennas and Propagation for Wireless Communication Systems*, 2nd Edn.. Chichester, West Sussex, England: John Wiley & Sons.
32. Votis C, Tatsis G and Kostarakis P (2010) Envelope correlation parameter measurements in a MIMO antenna array configuration. *International Journal of Communications, Network and System Sciences* **3**, 350–354.
33. Foegelle MD (2012) MIMO device performance measurements in a wireless environment simulator. *IEEE Electromagnetic Compatibility* **1**, 123–130.
34. Keysight Technologies (2014) *MIMO performance and condition Number in LTE test*. Application Note.
35. Tse D and Viswanath P (2005) *Fundamentals of Wireless Communication*. Cambridge: Cambridge University Press.
36. National Instruments (2017) Specifications USRP-2944 software defined radio reconfigurable device. Available at <http://www.ni.com/pdf/manuals/375724b.pdf> (Accessed 1 April 2020).



antenna arrays and wireless communication systems.

Grzegorz Bogdan received his M.Sc. and Ph.D. degrees in telecommunications from the Warsaw University of Technology (WUT), Poland in 2013 and 2019, respectively. Since 2019 he is an Assistant Professor at WUT in the Institute of Radioelectronics and Multimedia Technology of the Faculty of Electronics and Information Technology. His main research interests are the design and optimization of adaptive



Konrad Godziszewski received his Ph.D. degree in telecommunications from the Warsaw University of Technology (WUT), Poland in 2018. He joined the Institute of Radioelectronics and Multimedia Technology, WUT, in 2013 where he is currently an Assistant Professor. His current research interests include antennas, material characterization in sub-terahertz frequency range, and ferroelectric materials.



Yevhen Yashchyshyn received the M.E. degree from Lviv Polytechnic National University, Lviv, Ukraine, in 1979, the Ph.D. degree from Moscow Institute of Electronics and Mathematics (MIEM), Moscow, Russia, in 1986, and the D.Sc. (Habilitation) degree from Warsaw University of Technology (WUT), Warsaw, Poland, in 2006. In 2016, he was promoted to a Professor Title. Since 1999 he has been with the Institute of

Radioelectronics and Multimedia Technology, WUT, where he is currently a

Professor. He has authored over 250 technical papers, authored or co-authored five books, and holds a few patents. His current research interests include antenna theory and techniques, smart beamforming, reconfigurable antennas, radio over fiber techniques, and materials characterization, including ferroelectric ceramic-polymers composites investigation up to subterahertz frequency. In 2008, Professor Yashchyshyn was the recipient of the First Prize of EuMA at the 11th European Microwave Week, Amsterdam, the Netherlands, for his new concept of the reconfigurable antenna.